Point-contact Andreev reflection spectroscopy on the misfit phase superconductors $(PbSe)_{1.12}(TaSe_2)$ doped with Cl or Br

Liqiang Che,[1,2] Tian Le,[1,2] Qi Huang,[1,2] Lichang Yin,[1,2] Ye Chen,[1] Xiaohui Yang,[2] Zhu-An Xu,[2,3,4] and Xin Lu[1,2,3,4,*]

[1]*Center for Correlated Matter, Zhejiang University, Hangzhou 310058, China*

[2]*Department of Physics, Zhejiang University, Hangzhou 310027, China*

[3]*Zhejiang Province Key Laboratory of Quantum Technology and Device, Zhejiang University, Hangzhou 310027, China*

[4]*Collaborative Innovation Center of Advanced Microstructures, Nanjing University, Nanjing 210093, China*

(Received 24 October 2018; revised manuscript received 14 December 2018; published 22 January 2019)

We report point-contact Andreev reflection spectroscopy studies on possible topological superconductor candidates Cl- (Br-) doped $(PbSe)_{1.12}(TaSe_2)$ with superconducting transition temperature $T_c \sim 1.2$ K. A common double-peak feature is observed for the conductance curves at low temperature in the absence of a zero-bias conductance peak. We analyze conductance curves with the Blonder-Tinkham-Klapwijk model and the extracted superconducting gap follows a typical Bardeen-Cooper-Schrieffer temperature- and field-dependent behavior, with $2\Delta_0/k_BT_c \approx 3.7$ and 3.8 for Cl and Br doping, respectively. Our results strongly suggest that both Cl- and Br-doped $(PbSe)_{1.12}(TaSe_2)$ are fully gapped superconductors in an intermediate-coupling regime.

DOI: 10.1103/PhysRevB.99.024512

Majorana fermion, identical to its own antiparticle, has attracted intensive attention in condensed matter physics, due to its potential application in fault-tolerant quantum computations [1–4]. Topological superconductors (TSCs) have been proposed as a promising platform to host Majorana fermions in the form of Bogoliubov quasiparticles, where the nontrivial topology of the bulk superconductivity (SC) yields gapless Andreev bound states only at its surface/edge or topological defects. Despite the fact that various superconducting compounds are claimed to be intrinsic TSCs such as Sr_2RuO_4 [5], $Cu_xBi_2Se_3$ [6], $Cu_x(PbSe)_5(Bi_2Se_3)_6$ [7,8], and $PdTe_2$ [9,10], whose exact topological nature remains controversial, it is generally difficult to simultaneously achieve both nontrivial topology and superconductivity for the same compound. One strategy is to integrate distinct compounds with respective ingredients of TSC into an artificial hybrid device, where TSC emerges at the interface via superconducting proximity effect. For example, one-dimensional (1D) semiconducting nanowire/2D semiconducting film with strong spin-orbit coupling or 3D topological insulators are engineered in contact with an *s*-wave superconductor, such as InSb/Nb, InAs/Al, and InSb/NbTiN devices, and fully gapped superconductivity is induced at the interface due to the proximity effect [11–23]. A zero-bias tunneling conductance peak (ZBCP) in magnetic field has been observed at the surface/edge/vortex core as a signature of Majorana zero modes in these heterostructures [11–24].

Some misfit compounds are natural heterostructures with alternative stacking of topological and superconducting layers, serving as a good candidate to realize TSC at the heterostructure interfaces. Among them, a group of planar intergrowth compounds consist of an alternating rocksalt double-layer MX and transition metal dichalcogenide TX_2 sheets, described as $(MX)_{1+\delta}(TX_2)_m$, where M is Sn, Pb, Sb, Bi, or lanthanide; T is Ti, V, Nb, Ta, or Cr; and X is S or Se with $m = 1$–3. The MX and TX_2 layers match in one crystallographic axis but are incommensurate in the other axis, resulting in a nonstoichiometry in the formula with $0.08 < \delta < 0.28$ [25–27]. In this series, $(PbS)_{1.13}(TaS_2)$, $(BiS)_{1.07}(TaS_2)$, $(SnSe)_{1.18}(TiSe_2)_2$, $(PbSe)_{1.14}(TiSe_2)_n$ ($n = 1$, 2, 3), $(BiSe)_{1.10}(NbSe_2)$, $(LaSe)_{1.14}(NbSe_2)_2$, $(PbSe)_{1.14}(NbSe_2)_n$, and $(SnSe)_{1.16}(NbSe_2)$ have been reported to display exotic superconductivity [28–32]. It has been confirmed that charge-density-wave (CDW) in most bulk TX_2 is suppressed in the corresponding misfit compounds while SC is induced due to the charge transfer from the MX to TX_2 layers. In particular, the Sn-doped misfit compound $(Pb_{1-x}Sn_xSe)_{1.14}(TiSe_2)_2$ for $0 \leqslant x \leqslant 0.6$ displays a SC dome with the maximum T_c of 4.5 K at $x = 0.2$ [33,34]. Interestingly, its building block PbSe in bulk form is a trivial semiconductor while $Pb_{1-x}Sn_xSe$ with Sn substitution $x \geqslant 0.23$ becomes topological crystalline insulator with topological surface states [35,36]. Moreover, a PbSe monolayer is predicted to be a 2D topological crystalline insulator, which also owns a topological surface state protected by crystal symmetry [37]. It is thus promising to explore possible TSC in the $(PbSe)_{1+\delta}(TX_2)_m$ misfit phase superconductors with a natural presence of topology and SC heterostructures. Meanwhile, the corresponding transition-metal dichalcogenide TX_2 serves as an interesting platform to explore superconductivity and charge-density waves and their intricate relationship [38,39]. Recently, a similar series of misfit compounds $(PbSe)_{1.12}(TaSe_2)$ with 8% Cl (Br) substitution of the Se atoms are reported to be superconducting with $T_c \sim 1.2$ K and can be referred to as $Pb_{1.12}Ta(Se_{0.92}T_{0.08})_{3.12}$ (T = Cl and Br) [40]. It is desirable to have careful studies on its superconductivity and possible topological nature.

*Corresponding author: xinluphy@zju.edu.cn

In this article, we present a detailed point-contact Andreev reflection spectroscopy (PCARS) study on $Pb_{1.12}Ta(Se_{0.92}T_{0.08})_{3.12}$ (T = Cl and Br) single crystals (referred to as PSTS-Cl and PSTS-Br hereafter, respectively). A typical double-peak structure is observed in PCARS conductance curves for both compounds in the absence of a zero-bias conductance peak. A single superconducting gap Δ with $2\Delta_0/k_BT_c$ close to 3.8 is obtained when the data are fitted by the standard Blonder-Tinkham-Klapwijk (BTK) model and the gap Δ follows a conventional Bardeen-Cooper-Schrieffer (BCS) behavior as a function of either temperature or magnetic field.

PSTS-Cl and PSTS-Br single crystals with a typical size of 3×4 mm^2 were grown by the chemical vapor transport method using $PbBr_2$ or $PbCl_2$ as the chemical agent, while detailed procedures were described elsewhere [40]. Electrical resistivity measurements in zero magnetic field confirm the onset superconducting transition temperatures $T_c \sim 1.25$ and 1.20 K, respectively, as in Figs. 1(c) and 1(e). The single crystal x-ray diffraction patterns of PSTS-Cl and PSTS-Br single crystals are plotted in Fig. 1(b) with a full width at half maximum of all peaks about 0.05° as evidenced in the inset of Fig. 1(b). Due to distinct doping elements, the peaks of PSTS-Cl slightly shift toward the higher angles. Instead of the standard needle-anvil type, soft point-contact Andreev reflection spectroscopy was employed to study both samples from the same batch as in the resistivity, where a drop of Ag conductive paint was attached to the freshly cleaved sample surface with a 25-μm-diameter platinum wire in ambient atmosphere. In such a configuration, contact resistance comes from thousands of parallel channels of Ag grains in nanoscale contact and the conductance curve as a function of bias voltage, $G(V)$, was measured by the conventional lock-in technique. A sorption pumped He3 insert from Oxford Instruments was used to cool down to 300 mK and magnetic field can be applied along the sample's c axis above its upper critical field.

Figures 1(c) and 1(e) show the temperature dependence of zero-bias conductance, $G_0(T)$, for PCARS on PSTS-Cl and PSTS-Br single crystals, respectively. The kink at 1.2 K in $G_0(T)$ suggests a same T_c with that from the electrical resistivity, indicative of nondegradation of the cleaved surface. Figures 1(d) and 1(f) show several representative conductance $G(V)$ curves for contacts at 0.3 K of 10 contacts measured on different PSTS-Cl and PSTS-Br samples. We note that for the contacts on PSTS-Cl, no dip structure in $G(V)$ due to local heating effect is present with the bias voltage up to 0.8 mV, confirming contacts in the ballistic limit. However, for PSTS-Br, the dip structure in $G(V)$ indicates the contacts not in a pure Sharvin limit and that a heating effect cannot be avoided for our contacts on PSTS-Br. The $G(V)$ curves show two symmetric peaks around the bias voltage ≈0.2 mV and the SC gap Δ can be roughly estimated to be around 0.2 meV at 0.3 K. In order to quantitatively analyze the SC gap, we adopt the widely accepted Blonder-Thinkham-Klapwijk model with three parameters including the superconducting gap Δ, the tunneling barrier parameter Z and the quasiparticle broadening parameter Γ. At the lowest temperature, the $G(V)$ curves for PSTS-Cl can be well fitted by the BTK model as shown in Fig. 1(d), while a systematic deviation appears in the case of PSTS-Br due to the dip structure. We stress that the absence of a ZBCP in $G(V)$ probably implies a full SC gap without Andreev bound states from the nodal gap for either PSTS-Cl or PSTS-Br as discussed later.

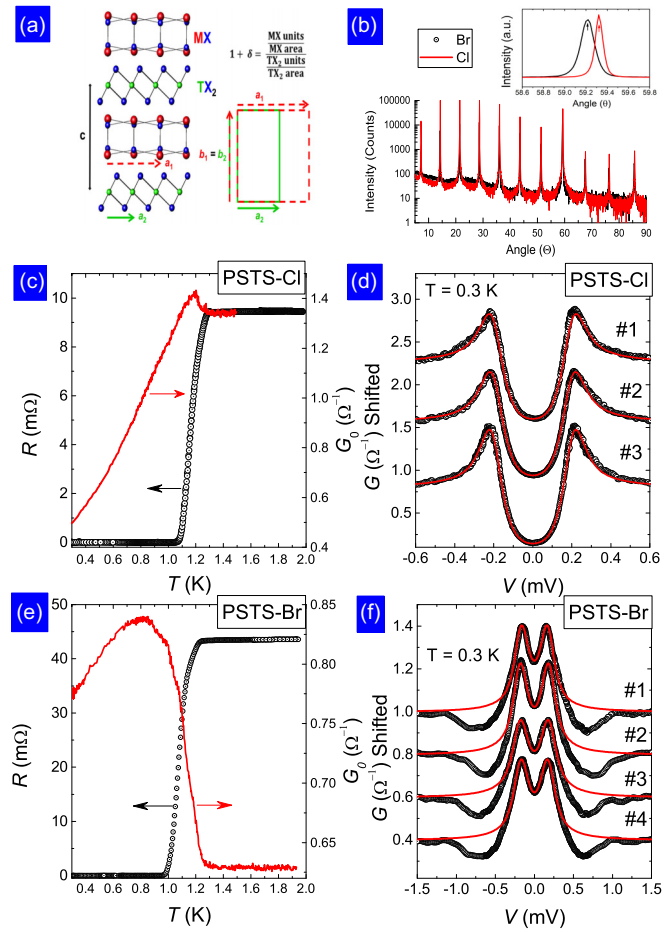

FIG. 1. (a) Schematic illustration of the crystal structure for the misfit phase compound $(PbSe)_{1.12}TaSe_2$ adapted from Ref. [41]; (b) Single crystal x-ray diffraction of PSTS-Cl and PSTS-Br in the [001] direction, suggesting an effective doping of Cl and Br into $(PbSe)_{1.12}TaSe_2$; [(c) and (e)] the temperature dependence of point-contact zero-bias conductance $G_0(T)$ in comparison with the electrical resistivity for PSTS-Cl and PSTS-Br, respectively. [(d) and (f)] Representative point-contact conductance curves $G(V)$ at 0.3 K for PSTS-Cl and PSTS-Br, respectively. The curves are shifted vertically for clarity and solid lines are the optimal BTK fitting curves.

Figure 2(a) plots one representative set of the normalized conductance curves as a function of temperature for Soft PCARS on PSTS-Cl, with their optimal BTK fitting curves for comparison. With increased temperature, the Andreev reflection intensity is reduced and the distance between double peaks decreases and finally disappears above T_c. The temperature-dependent SC gap Δ extracted from the BTK fitting is shown in Fig. 2(b) and it follows the conventional BCS temperature behavior. The SC gap Δ is extrapolated to be 0.20 meV at 0 K and it closes at the critical temperature $T_c = 1.25$ K, yielding $2\Delta(0)/k_BT_c = 3.8$ slightly larger than the weak-coupling-limit value 3.52. Meanwhile, the ratio between quasiparticle smearing parameter Γ and superconducting gap

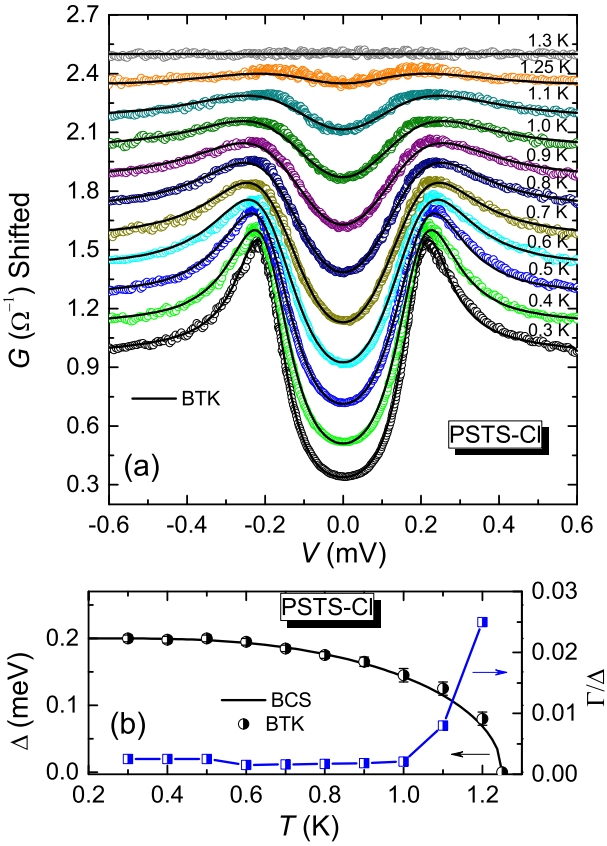

FIG. 2. (a) Temperature evolution of soft point-contact conductance curves $G(V)$ of PSTS-Cl (open symbols) in comparison with their optimal BTK fitting curves with $Z = 1.3$ (solid lines). (b) The superconducting gap as a function of temperature $\Delta(T)$ (half-filled circles) follows the BCS behavior (solid line) while the ratio between the smearing parameter Γ and superconducting gap Δ, Γ/Δ increases dramatically close to T_c (blue squares).

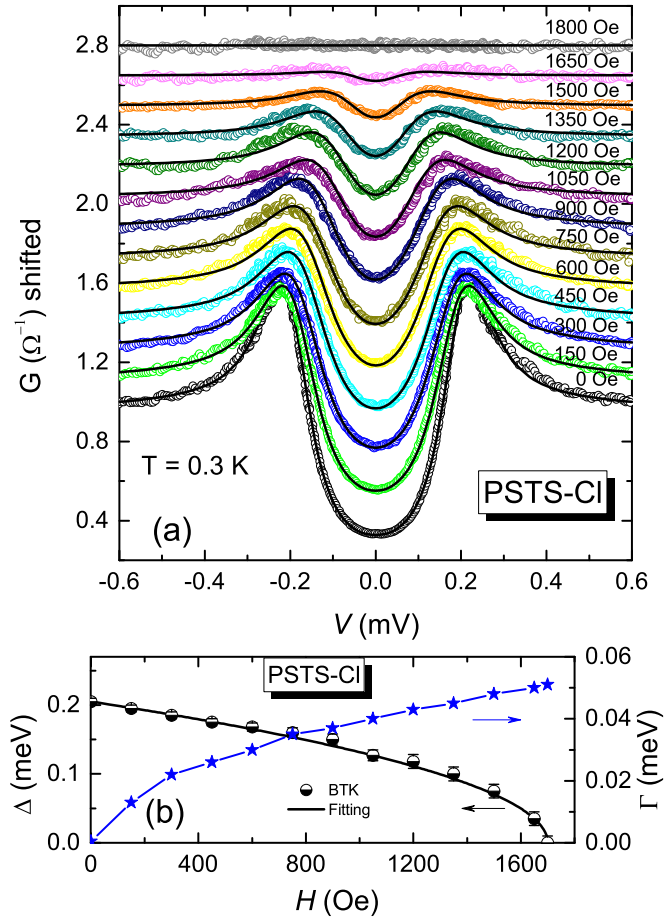

FIG. 3. (a) Magnetic field evolution of soft point-contact conductance $G(V)$ of PSTS-Cl (open symbols) at 0.3 K with the field in the [001] direction. The curves are shifted for clarity and compared with their optimal BTK fitting curves (solid lines). (b) The extracted superconducting gap as a function of field $\Delta(H)$ (half-filled circles) is consistent with the theoretical predicted behavior (solid line), while the smearing parameter Γ (blue stars) increases as a function of magnetic field.

Δ as a function of temperature is plotted in Fig. 2(b) and it increases dramatically close to T_c due to enhanced pair-breaking effect. At the lowest temperature $T = 0.3$ K, the fitting parameter Γ/Δ can be as low as 0.0025, signaling a very small gap distribution, if any. It is thus likely that PSTS-Cl is a single full-gap superconductor in the intermediate-coupling regime.

A full SC gap in PSTS-Cl is also corroborated by its behavior in a magnetic field. Figure 3(a) shows the field dependence of its point-contact spectra at the lowest temperature $T = 0.3$ K, where the magnetic field is applied perpendicular to the ab plane. With increased field, the double-peak structure is gradually suppressed and it completely vanishes with $H \approx 0.17$ T. From BTK fitting, the extracted superconducting gap follows the typical magnetic behavior for a type-II superconductor in its vortex state [42], complying with $\Delta = \Delta_0(1 - H/H_{c2})^{1/2}$ as shown in Fig. 3(b). The quasiparticle smearing parameter Γ monotonically increases when ramping up the field as in Fig. 3(b), caused by the pair-breaking effect with increased vortex density in the contact area.

A comparative PCARS study on PSTS-Br is performed with the spectra evolution as a function of temperature and magnetic field shown in Figs. 4(a) and 4(b), respectively. Its point-contact spectra can also be well fitted except for the dip region by a single-gap BTK model with $\Delta = 0.19$ meV at 0.3 K, supporting a conventional full-gap superconductor in PSTS-Br. We notice a systematic difference for the tunneling barrier parameter Z between PSTS-Cl and PSTC-Br (roughly 1.1 and 0.4, respectively). $Z_{\mathrm{Cl}} > Z_{\mathrm{Br}}$ implies a much larger interface tunneling barrier strength for PSTS-Cl than that for PSTS-Br. We speculate that the exposed surface layer after cleaving is different for these compounds, which terminate at the insulating $PbSe_{1-x}T_x$ layer for PSTS-Cl while it ends at the metallic TX_2 layer for PSTC-Br, yielding different barrier strengths for soft point contacts. The exact origin of distinct tunneling barrier in PSTS still remains an open issue and careful characterizations of the cleaved surface are necessary in the future.

Our PCARS results suggest a full SC gap for both PSTS-Cl and PSTS-Br, which is essential to realize topological superconductivity [43]. Further exploration on the spin-polarized density of states in the vortex core by STM should be informative to identify the possible existence of Majorana zero modes,

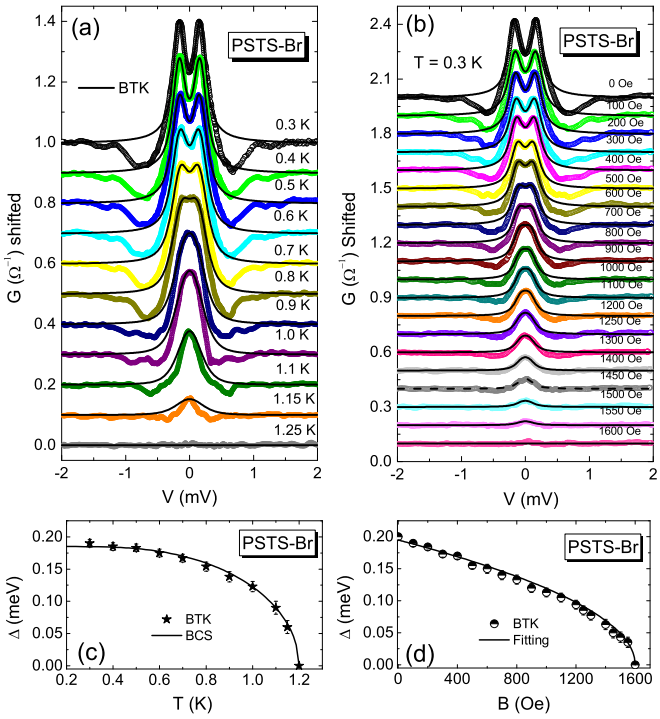

FIG. 4. [(a) and (b)] Temperature and magnetic field evolution of one representative set of PCARS data on PSTS-Br (open symbols) in comparison with their optimal BTK fitting curves with $Z = 0.43$ (solid lines). The conductance curves are shifted for clarity and the magnetic filed is applied in the [001] direction at 0.3 K. [(c) and (d)] The extracted superconducting gap Δ from BTK model as a function of temperature and magnetic field, respectively. The gap Δ follows the theoretical predicted behaviors in both cases (solid lines).

while it is challenging for PCARS to observe the ZBCP localized in the vortex core due to its lack of spacial resolution. We also note that, for these misfit compounds, charge transfer has been commonly observed at the interfaces from the MX to TX_2 layers. In the case of $(PbSe)_{1.16}(TiSe_2)_2$, electrons in the fully occupied valence band of PbSe come mostly from Se $4p$ orbitals and are partially transferred to the empty conduction band of $TiSe_2$ derived from the Ti $3d$ orbitals, changing both semiconducting layers to be metallic [31,44]. Due to the charge transfer in this natural heterostructure, it is likely that the PbSe layer can no longer be viewed as a topological crystalline insulator. Instead, the charge transfer from PbSe to $TaSe_2$ may act as electron doping into $TaSe_2$, tuning $TaSe_2$ layers into a superconducting state as in the bulk form. Another possible scenario for the bulk superconductivity in $TaSe_2$ layers is due to enhanced surface-volume ratio with the alternating stacking structure. Scanning tunneling conductance of the $TaSe_2$ crystal surface layers with $2H$ structure shows a superconducting gap with a critical temperature around 1 K, much higher than its bulk $T_c \sim 0.15$ K [48].

On the other hand, if the nontrivial topology of PbSe layers remains intact, the surface states at the top and bottom interfaces for the same $TaSe_2$ block will probably hybridize with each other due to their proximity in distance, resulting in a hybridization gap and preventing the emergence of Majorana zero modes. Such a hybridization effect has been reported in an angle-resolved photoemission study on $(PbSe)_5(Bi_2Se_3)_{3m}$ with $m = 2$, another natural heterostructure consisting of alternating topological and ordinary insulating layers [45–47]. A gapped Dirac-cone state was observed and explained by the hybridization between top and bottom topological states of Bi_2Se_3 slabs, similarly to a typical Rashba system. Increasing the thickness of the encapsulated Bi_2Se_3 slab with a larger m has proven to eliminate the hybridization effect and to recover the topological surface state.

To summarize, our PCARS measurements on the misfit phase superconductors $Pb_{1.12}Ta(Se_{0.92}T_{0.08})_{3.12}$ (T = Cl and Br) reveal a typical double-peak structure in $G(V)$ curves without a zero-bias conductance peak. Point-contact $G(V)$ curves can be well fitted by the BTK model and the extracted superconducting gap $\Delta_0 = 0.19$ meV (0.20 meV) for PSTS-Cl (PSTS-Br) gives $2\Delta/k_BT_c \approx 3.7$ (3.8) in the intermediate coupling regime, following the conventional BCS temperature and magnetic field dependence. Further studies are required to address its exact topological nature of the superconductivity in this $Pb_{1.12}Ta(Se_{0.92}T_{0.08})_{3.12}$ series.

We are grateful for valuable discussions with Y. Zhou and H. Q. Yuan. Work at Zhejiang University is supported by National Key R & D Program of China (Grants No. 2016YFA0300402 and No. 2017YFA0303101) and the National Natural Science Foundation of China (Grants No. 11674279, No. 11774305, No. 11604291, and No. 11374257). X.L. acknowledges support from the Zhejiang Provincial Natural Science Foundation of China (LR18A04001).

[1] E. Majorana, Teoria simmetrica dell'elettrone e del positrone, Nuovo Cim. **14**, 171 (1937).
[2] C. W. J. Beenakker, Search for majorana fermions in superconductors, Annu. Rev. Condens. Matter Phys. **4**, 113 (2013).
[3] C. Nayak, S. H. Simon, A. Stern, M. Freedman, and S. Das Sarma, Non-Abelian anyons and topological quantum computation, Rev. Mod. Phys. **80**, 1083 (2008).
[4] A.Y. Kitaev, Fault-tolerant quantum computation by anyons, Ann. Phys. **303**, 2 (2003).
[5] S. Das Sarma, C. Nayak, and S. Tewari, Proposal to stabilize and detect half-quantum vortices in strontium ruthenate thin films: Non-abelian braiding statistics of vortices in a $p_x + ip_y$ superconductor, Phys. Rev. B **73**, 220502 (2006).
[6] L. Fu and E. Berg, Odd-Parity Topological Superconductors: Theory and Application to $Cu_xBi_2Se_3$, Phys. Rev. Lett. **105**, 097001 (2010).
[7] S. Sasaki, K. Segawa, and Y. Ando, Superconductor derived from a topological insulator heterostructure, Phys. Rev. B **90**, 220504 (2014).
[8] K. Nakayama, H. Kimizuka, Y. Tanaka, T. Sato, S. Souma, T. Takahashi, S. Sasaki, K. Segawa, and Y. Ando, Observation of two-dimensional bulk electronic states in the superconducting

topological insulator heterostructure $Cu_x(PbSe)_5(Bi_2Se_3)_6$: Implications for unconventional superconductivity, Phys. Rev. B **92**, 100508 (2015).

[9] H. J. Noh, J. Jeong, E. J. Cho, K. Kim, B. I. Min, and B. G. Park, Experimental Realization of Type-II Dirac Fermions in a $PdTe_2$ Superconductor, Phys. Rev. Lett. **119**, 016401 (2017).

[10] Y. Liu, J. Z. Zhao, L. Yu, C. T. Lin, A. J. Liang, C. Hu, Y. Ding, Y. Xu, S. L. He, L. Zhao, G. D. Liu, X. L. Dong, J. Zhang, C. T. Chen, Z. Y. Xu, H. M. Weng, X. Dai, Z. Fang, and X. J. Zhou, Identification of topological surface state in $PdTe_2$ superconductor by angle-resolved photoemission spectroscopy, Chin. Phys. Lett. **32**, 067303 (2015).

[11] L. P. Rokhinson, X. Y. Liu, and J. K. Furdyna, The fractional a.c. Josephson effect in a semiconductor-superconductor nanowire as a signature of Majorana particles, Nat. Phys. **8**, 795 (2012).

[12] A. Das, Y. Ronen, Y. Most, Y. Oreg, M. Heiblum, and H. Shtrikman, Zero-bias peaks and splitting in an Al-InAs nanowire topological superconductor as a signature of majorana fermions, Nat. Phys. **8**, 887 (2012).

[13] H. Zhang, Ö. Gül, S. Conesa-Boj, M. P. Nowak, M. Wimmer, K. Zuo, V. Mourik, F. K. de Vries, J. van Veen, M. W. A. de Moor, J. D. S. Bommer, D. J. van Woerkom, D. Car, S. R. Plissard, E. P. A. M. Bakkers, M. Quintero-Pérez, M. C. Cassidy, S. Koelling, S. Goswami, K. Watanabe, T. Taniguchi, and L. P. Kouwenhoven, Ballistic superconductivity in semiconductor nanowires, Nat. Commun. **8**, 16025 (2017).

[14] A. Y. Kitaev, Unpaired majorana fermions in quantum wires, Phys.-Usp. **44**, 131 (2001).

[15] N. B. Kopnin and M. M. Salomaa, Mutual friction in superfluid ^{3}He: Effects of bound states in the vortex core, Phys. Rev. B **44**, 9667 (1991).

[16] Y. Oreg, G. Refael, and F. von Oppen, Helical Liquids and Majorana Bound States in Quantum Wires, Phys. Rev. Lett. **105**, 177002 (2010).

[17] R. M. Lutchyn, J. D. Sau, and S. Das Sarma, Majorana Fermions and a Topological Phase Transition in Semiconductor-Superconductor Heterostructures, Phys. Rev. Lett. **105**, 077001 (2010).

[18] J. D. Sau, R. M. Lutchyn, S. Tewari, and S. Das Sarma, Generic New Platform for Topological Quantum Computation Using Semiconductor Heterostructures, Phys. Rev. Lett. **104**, 040502 (2010).

[19] J. D. Sau, S. Tewari, R. M. Lutchyn, T. D. Stanescu, and S. Das Sarma, Non-abelian quantum order in spin-orbit-coupled semiconductors: Search for topological majorana particles in solid-state systems, Phys. Rev. B **82**, 214509 (2010).

[20] J. Alicea, Majorana fermions in a tunable semiconductor device, Phys. Rev. B **81**, 125318 (2010).

[21] L. Fu and C. L. Kane, Superconducting Proximity Effect and Majorana Fermions at the Surface of a Topological Insulator, Phys. Rev. Lett. **100**, 096407 (2008).

[22] J. P. Xu, C. H. Liu, M. X. Wang, J. F. Ge, Z. L. Liu, X. J. Yang, Y. Chen, Y. Liu, Z. A. Xu, C. L. Gao, D. Qian, F. C. Zhang, and J. F. Jia, Artificial Topological Superconductor by the Proximity Effect, Phys. Rev. Lett. **112**, 217001 (2014).

[23] H. H. Sun, K. W. Zhang, L. H. Hu, C. Li, G. Y. Wang, H. Y. Ma, Z. A. Xu, C. L. Gao, D. D. Guan, Y. Y. Li, C. H. Liu, D. Qian, Y. Zhou, L. Fu, S. C. Li, F. C. Zhang, and J. F. Jia, Majorana Zero Mode Detected with Spin Selective Andreev Reflection in the Vortex of a Topological Superconductor, Phys. Rev. Lett. **116**, 257003 (2016).

[24] F. Pientka, G. Kells, A. Romito, P. W. Brouwer, and F. von Oppen, Enhanced Zero-Bias Majorana Peak in the Differential Tunneling Conductance of Disordered Multisubband Quantum-Wire/Superconductor Junctions, Phys. Rev. Lett. **109**, 227006 (2012).

[25] G. A. Wiegers, Misfit layer compounds: Structures and physical properties, Prog. Solid State Chem. **24**, 1 (1996).

[26] J. Rouxel, A. Meerschaut, and G. A. Wiegers, Chalcogenide misfit layer compounds, J. Alloys Compd. **229**, 144 (1995).

[27] W. Y. Zhou, A. Meetsma, J. L. de Boer, and G. A. Wiegers, Characterization, electrical transport and magnetic properties of the rare earth misfit layer compounds $(TbS)_{1.21}NbS_2$, $(TbS)_{1.20}TaS_2$, $(DyS)_{1.22}NbS_2$ and $(DyS)_{1.21}TaS_2$, J. Alloys Compd. **233**, 80 (1996).

[28] Y. Oosawa, Y. Gotoh, J. Akimoto, T. Tsunoda, M. Sohma, and M. Onoda, Three types of ternary selenides with layered composite crystal structures formed in the Pb-Nb-Se system, Jpn. J. Appl. Phys. **31**, L1096 (1992).

[29] R. Roesky, A. Meerschaut, J. Rouxel, and J. Chen, Structure and electronic transport properties of the misfit layer compound $(LaSe)_{1.14}(NbSe_2)_2$, $LaNb_2Se_5$, Z. anorg. allg. Chem **619**, 117 (1993).

[30] G. A. Wiegers and A. Meerschaut, Misfit layer compounds $(MS)_nTS_2$ (M = Sn, Pb, Bi, rare earth metals; T=Nb, Ta, Ti, V, Cr; $1.08 < n < 1.23$): Structures and physical properties, Mater. Sci. Forum **100**, 101 (1992).

[31] Q. Yao, D. W. Shen, C. H. P. Wen, C. Q. Hua, L. Q. Zhang, N. Z. Wang, X. H. Niu, Q. Y. Chen, P. Dudin, Y. H. Lu, Y. Zheng, X. H. Chen, X. G. Wan, and D. L. Feng, Charge Transfer Effects in Naturally Occurring Van Der Waals Heterostructures $(PbSe)_{1.16}(TiSe_2)_m$ ($m = 1, 2$), Phys. Rev. Lett. **120**, 106401 (2018).

[32] H. Bai, X. H. Yang, Y. Liu, M. Zhang, M. M. Wang, Y. P. Li, J. Ma, Q. Tao, Y. W. Xie, G. H. Cao, and Z. A. Xu, Superconductivity in a misfit layered compound $(SnSe)_{1.16}(NbSe_2)$, J. Phys.: Condens. Matter **30**, 355701 (2018).

[33] H. X. Luo, K. Yan, I. Pletikosic, W. W. Xie, B. F. Phelan, T. Valla, and R. J. Cava, Superconductivity in a misfit phase that combines the topological crystalline insulator $Pb_{1-x}Sn_xSe$ with the CDW-bearing transition metal dichalcogenide $TiSe_2$, J. Phys. Soc. Jpn. **85**, 064705 (2016).

[34] N. Giang, Q. Xu, Y. S. Hor, A. J. Williams, S. E. Dutton, H. W. Zandbergen, and R. J. Cava, Superconductivity at 2.3 K in the misfit compound $(PbSe)_{1.16}(TiSe_2)_2$, Phys. Rev. B **82**, 024503 (2010).

[35] P. J. Lin and L. Kleinman, Energy bands of PbTe, PbSe, and PbS, Phys. Rev. **142**, 478 (1966).

[36] P. Dziawa, B. J. Kowalski, K. Dybkod, R. Buczko, A. Szczerbakow, M. Szot, E. Lusakowska, T. Balasubramanian, B. M. Wojek, M. H. Berntsen, O. Tjernberg, and T. Story, Topological crystalline insulator states in $Pb_{1-x}Sn_xSe$, Nat. Mater. **11**, 1023 (2012).

[37] E. O. Wrasse and T. M. Schmidt, Prediction of two-dimensional topological crystalline insulator in PbSe monolayer, Nano. Lett. **14**, 5717 (2014).

[38] D. C. Freitas, P. Rodière, M. R. Osorio, E. Navarro-Moratalla, N. M. Nemes, V. G. Tissen, L. Cario, E. Coronado,

M. García-Hernández, S. Vieira, M. Núñez-Regueiro, and H. Suderow, Strong enhancement of superconductivity at high pressures within the charge-density-wave states of 2H−TaS_2 and 2H−$TaSe_2$, Phys. Rev. B **93**, 184512 (2016).

[39] H. X. Luo, W. W. Xie, J. Tao, I. Pletikosic, T. Valla, G. S. Sahasrabudhe, G. Osterhoudt, E. Sutton, K. S. Burch, E. M. Seibel, J. W. Krizan, Y. M. Zhu, and R. J. Cava, Differences in chemical doping matter: Superconductivity in $Ti_{1-x}Ta_xSe_2$ but not in $Ti_{1-x}Nb_xSe_2$, Chem. Mater. **28**, 1927 (2016).

[40] X. H. Yang, M. M. Wang, Y. P. Li, H. Bai, J. Ma, X. K. Sun, Q. Tao, C. Dong, and Z. A. Xu, Superconductivity in a misfit compound $(SnSe)_{1.12}(TaSe_2)$, Supercond. Sci. Technol. **31**, 5010 (2018).

[41] D. R. Merrill, D. B. Moore, S. R. Bauers, M. Falmbigl, and D. C. Johnson, Misfit layer compounds and ferecrystals: Model systems for thermoelectric nanocomposites, Materials **8**, 2000 (2015).

[42] E. H. Brandt, Microscopic theory of clean type-II superconductors in the entire field-temperature plane, Phys. Stat. Sol B **77**, 105 (1976).

[43] M. Sato and Y. Ando, Topological superconductors: A review, Rep. Prog. Phys. **80**, 076501 (2017).

[44] S. R. Bauers, J. Ditto, D. B. Moore, and D. C. Johnson, Structure–property relationships in non-epitaxial chalcogenide heterostructures: The role of interface density on charge exchange, Nanoscale **8**, 14665 (2016).

[45] L. Fang, C. C. Stoumpos, Y. Jia, A. Glatz, D. Y. Chung, H. Claus, U. Welp, W.-K. Kwok, and M. G. Kanatzidis, Dirac fermions and superconductivity in the homologous structures $(Ag_xPb_{1-x}Se)_5(Bi_2Se_3)_{3m}$ ($m = 1, 2$), Phys. Rev. B **90**, 020504 (2014).

[46] M. G. Kanatzidis, Structural evolution and phase homologies for "design" and prediction of solid-state compounds, Acc. Chem. Res. **38**, 359 (2005).

[47] K. Nakayama, K. Eto, Y. Tanaka, T. Sato, S. Souma, T. Takahashi, K. Segawa, and Y. Ando, Manipulation of Topological States and the Bulk Band Gap Using Natural Heterostructures of a Topological Insulator, Phys. Rev. Lett. **109**, 236804 (2012).

[48] J. A. Galvis, P. Rodière, I. Guillamon, M. R. Osorio, J. G. Rodrigo, L. Cario, E. Navarro-Moratalla, E. Coronado, S. Vieira, and H. Suderow, Scanning tunneling measurements of layers of superconducting 2H−$TaSe_2$: Evidence for a zero-bias anomaly in single layers, Phys. Rev. B **87**, 094502 (2013).